Research Article | Vol. 25, No. 8 | 17 Apr 2017 | OPTICS EXPRESS 9262

Optics EXPRESS

# Hot luminescence from gold nanoflowers and its application in high-density optical data storage

YUNBAO ZHENG,[1] HAIYING LIU,[1] JIN XIANG,[1] QIAOFENG DAI,[1] MIN OUYANG,[1] SHAOLONG TIE,[2] AND SHENG LAN[1,*]

[1]*Provincial Key Laboratory of Nanophotonic Functional Materials and Devices, School of Information and Optoelectronic Science and Engineering, South China Normal University, Guangzhou 510006, China*

[2]*School of Chemistry and Environment, South China Normal University, Guangzhou 510006, China*

[*]*slan@scnu.edu.cn*

**Abstract:** Gold nanoflowers with feature sizes ranging from several tenths to several hundred nanometers were synthesized by using the one-pot method. They were formed by the self-organization of gold nanoparticles of several nanometers and exhibited broad extinction spectra in the near infrared spectral range. Randomly distributed hot spots originating from the strongly localized modes were generated in gold nanoflowers and their appearances exhibited strong dependences on both the polarization and wavelength of the excitation light. Under the excitation of femtosecond laser pulses, such hot spots emitted efficient hot luminescence spanning the visible to near infrared spectral range. Distinct from the hot luminescence of single hot spots formed on rough gold and silver surfaces, the hot luminescence from gold nanoflowers composed of a large number of hot spots exhibited excitation-intensity dependence quite similar to the emission spectrum. It was demonstrated that the polarization- and wavelength-dependent hot luminescence of gold nanoflowers can be utilized to realize optical data storage with high density and low energy.



**OCIS codes:** (260.3800) Luminescence; (160.4236) Nanomaterials; (210.0210) Optical data storage.

## References and links

1. P. N. Prasad, *Nanophotonics* (John Wiley & Sons, 2004).
2. M. C. Daniel and D. Astruc, "Gold nanoparticles: assembly, supramolecular chemistry, quantum-size-related properties, and applications toward biology, catalysis, and nanotechnology," Chem. Rev. **104**(1), 293–346 (2004).
3. S. Nie and S. R. Emory, "Probing Single Molecules and Single Nanoparticles by Surface-Enhanced Raman Scattering," Science **275**(5303), 1102–1106 (1997).
4. X. Huang, I. H. El-Sayed, W. Qian, and M. A. El-Sayed, "Cancer Cells Assemble and Align Gold Nanorods Conjugated to Antibodies to Produce Highly Enhanced, Sharp, and Polarized Surface Raman Spectra: A Potential Cancer Diagnostic Marker," Nano Lett. **7**(6), 1591–1597 (2007).
5. X. Qian, X. H. Peng, D. O. Ansari, Q. Yin-Goen, G. Z. Chen, D. M. Shin, L. Yang, A. N. Young, M. D. Wang, and S. Nie, "In vivo tumor targeting and spectroscopic detection with surface-enhanced Raman nanoparticle tags," Nat. Biotechnol. **26**(1), 83–90 (2007).
6. Y. Sun and Y. Xia, "Shape-controlled synthesis of gold and silver nanoparticles," Science **298**(5601), 2176–2179 (2002).
7. A. R. Tao, S. Habas, and P. Yang, "Shape Control of Colloidal Metal Nanocrystals," Small **4**(3), 310–325 (2008).
8. S. E. Skrabalak, J. Chen, Y. Sun, X. Lu, L. Au, C. M. Cobley, and Y. Xia, "Gold Nanocages: Synthesis, Properties, and Applications," Acc. Chem. Res. **41**(12), 1587–1595 (2008).
9. T. K. Sau and A. L. Rogach, "Nonspherical Noble Metal Nanoparticles: Colloid-Chemical Synthesis and Morphology Control," Adv. Mater. **22**(16), 1781–1804 (2010).
10. M. Grzelczak, J. Vermant, E. M. Furst, and L. M. Liz-Marzán, "Directed Self-Assembly of Nanoparticles," ACS Nano **4**(7), 3591–3605 (2010).
11. S. C. Glotzer and M. J. Solomon, "Anisotropy of building blocks and their assembly into complex structures," Nat. Mater. **6**(7), 557–562 (2007).
12. M. B. Mohamed, V. Volkov, S. Link, and M. A. El-Sayed, "The 'lightning' gold nanorods: fluorescence enhancement of over a million compared to the gold metal," Chem. Phys. Lett. **317**(6), 517–523 (2000).

#285458 https://doi.org/10.1364/OE.25.009262
Journal © 2017 Received 30 Jan 2017; revised 6 Apr 2017; accepted 7 Apr 2017; published 12 Apr 2017

Optics EXPRESS


13. S. Link and M. A. El-Sayed, "Simulation of the Optical Absorption Spectra of Gold Nanorods as a Function of Their Aspect Ratio and the Effect of the Medium Dielectric Constant," J. Phys. Chem. B **109**(20), 10531–10532 (2005).
14. M. Gu, X. Li, and Y. Cao, "Optical storage arrays: a perspective for future big data storage," Light Sci. Appl. **3**(5), e177 (2014).
15. J. W. M. Chon, C. Bullen, P. Zijlstra, and M. Gu, "Spectral encoding on Gold Nanorods Doped in a Silica Sol–Gel Matrix and Its Application to High-Density Optical Data Storage," Adv. Funct. Mater. **17**(6), 875–880 (2007).
16. P. Zijlstra, J. W. Chon, and M. Gu, "Five-dimensional optical recording mediated by surface plasmons in gold nanorods," Nature **459**(7245), 410–413 (2009).
17. X. Li, T. H. Lan, C. H. Tien, and M. Gu, "Three-dimensional orientation-unlimited polarization encryption by a single optically configured vectorial beam," Nat. Commun. **3**, 998 (2012).
18. E. Hao and G. C. Schatz, "Electromagnetic fields around silver nanoparticles and dimers," J. Chem. Phys. **120**(1), 357–366 (2004).
19. J. R. Piper, V. Liu, and S. Fan, "Total absorption by degenerate critical coupling," Appl. Phys. Lett. **104**(25), 251110 (2014).
20. G. Baffou and R. Quidant, "Thermo-plasmonics: using metallic nanostructures as nano-sources of heat," Laser Photonics Rev. **7**(2), 171–187 (2013).
21. K. L. Wustholz, A.-I. Henry, J. M. McMahon, R. G. Freeman, N. Valley, M. E. Piotti, M. J. Natan, G. C. Schatz, and R. P. Van Duyne, "Structure-Activity Relationships in Gold Nanoparticle Dimers and Trimers for Surface-Enhanced Raman Spectroscopy," J. Am. Chem. Soc. **132**(31), 10903–10910 (2010).
22. P. Mühlschlegel, H. J. Eisler, O. J. Martin, B. Hecht, and D. W. Pohl, "Resonant optical antennas," Science **308**(5728), 1607–1609 (2005).
23. W. Zhang, L. Huang, C. Santschi, and O. J. Martin, "Trapping and sensing 10 nm metal nanoparticles using plasmonic dipole antennas," Nano Lett. **10**(3), 1006–1011 (2010).
24. L. Chen, G.-C. Li, G.-Y. Liu, Q.-F. Dai, S. Lan, S.-L. Tie, and H.-D. Deng, "Sensing the Moving Direction, Position, Size, and Material Type of Nanoparticles with the Two-Photon-Induced Luminescence of a Single Gold Nanorod," J. Phys. Chem. C **117**(39), 20146–20153 (2013).
25. G. Lu, L. Hou, T. Zhang, W. Li, J. Liu, P. Perriat, and Q. Gong, "Anisotropic Plasmonic Sensing of Individual or Coupled Gold Nanorods," J. Phys. Chem. C **115**(46), 22877–22885 (2011).
26. P. Zijlstra, P. M. Paulo, and M. Orrit, "Optical detection of single non-absorbing molecules using the surface plasmon resonance of a gold nanorod," Nat. Nanotechnol. **7**(6), 379–382 (2012).
27. L. Shao, C. Fang, H. Chen, Y. C. Man, J. Wang, and H. Q. Lin, "Distinct plasmonic manifestation on gold nanorods induced by the spatial perturbation of small gold nanospheres," Nano Lett. **12**(3), 1424–1430 (2012).
28. J.-X. Li, Y. Xu, Q.-F. Dai, S. Lan, and S.-L. Tie, "Manipulating light-matter interaction in a gold nanorod assembly by plasmonic coupling," Laser Photonics Rev. **10**(5), 826–834 (2016).
29. H. Wang, T. B. Huff, D. A. Zweifel, W. He, P. S. Low, A. Wei, and J. X. Cheng, "In vitro and in vivo two-photon luminescence imaging of single gold nanorods," Proc. Natl. Acad. Sci. U.S.A. **102**(44), 15752–15756 (2005).
30. K. Imura, T. Nagahara, and H. Okamoto, "Near-Field Two-Photon-Induced Photoluminescence from Single Gold Nanorods and Imaging of Plasmon Modes," J. Phys. Chem. B **109**(27), 13214–13220 (2005).
31. X.-F. Jiang, Y. Pan, C. Jiang, T. Zhao, P. Yuan, T. Venkatesan, and Q.-H. Xu, "Excitation Nature of Two-Photon Photoluminescence of Gold Nanorods and Coupled Gold Nanoparticles Studied by Two-Pulse Emission Modulation Spectroscopy," J. Phys. Chem. Lett. **4**(10), 1634–1638 (2013).
32. P. Biagioni, M. Celebrano, M. Savoini, G. Grancini, D. Brida, S. Mátéfi-Tempfli, M. Mátéfi-Tempfli, L. Duò, B. Hecht, G. Cerullo, and M. Finazzi, "Dependence of the two-photon photoluminescence yield of gold nanostructures on the laser pulse duration," Phys. Rev. B **80**(4), 045411 (2009).
33. T. Haug, P. Klemm, S. Bange, and J. M. Lupton, "Hot-Electron Intraband Luminescence from Single Hot Spots in Noble-Metal Nanoparticle Films," Phys. Rev. Lett. **115**(6), 067403 (2015).
34. K.-Q. Lin, J. Yi, S. Hu, J.-J. Sun, J.-T. Zheng, X. Wang, and B. Ren, "Intraband Hot-Electron Photoluminescence from Single Silver Nanorods," ACS Photonics **3**(7), 1248–1255 (2016).
35. X. Huang, S. Li, Y. Huang, S. Wu, X. Zhou, S. Li, C. L. Gan, F. Boey, C. A. Mirkin, and H. Zhang, "Synthesis of hexagonal close-packed gold nanostructures," Nat. Commun. **2**, 292 (2011).
36. M. A. Boles, M. Engel, and D. V. Talapin, "Self-Assembly of Colloidal Nanocrystals: From Intricate Structures to Functional Materials," Chem. Rev. **116**(18), 11220–11289 (2016).
37. C. A. Mirkin, R. L. Letsinger, R. C. Mucic, and J. J. Storhoff, "A DNA-based method for rationally assembling nanoparticles into macroscopic materials," Nature **382**(6592), 607–609 (1996).
38. S. Watanabe, Y. Mino, Y. Ichikawa, and M. T. Miyahara, "Spontaneous Formation of Cluster Array of Gold Particles by Convective Self-Assembly," Langmuir **28**(36), 12982–12988 (2012).
39. K. Yee, "Numerical solution of initial boundary value problems involving Maxwell's equations in isotropic media," IEEE Trans. Antenn. Propag. **14**(3), 302–307 (1966).
40. P. B. Johnson and R. W. Christy, "Optical constant of the noble metals," Phys. Rev. B **6**(12), 4370–4379 (1972).
41. S. Viarbitskaya, A. Teulle, R. Marty, J. Sharma, C. Girard, A. Arbouet, and E. Dujardin, "Tailoring and imaging the plasmonic local density of states in crystalline nanoprisms," Nat. Mater. **12**(5), 426–432 (2013).

Optics EXPRESS

42. P. Ghenuche, S. Cherukulappurath, T. H. Taminiau, N. F. van Hulst, and R. Quidant, "Spectroscopic Mode Mapping of Resonant Plasmon Nanoantennas," Phys. Rev. Lett. **101**(11), 116805 (2008).
43. D.-S. Wang, F.-Y. Hsu, and C.-W. Lin, "Surface plasmon effects on two photon luminescence of gold nanorods," Opt. Express **17**(14), 11350–11359 (2009).
44. M. L. Weber, J. P. Litz, D. J. Masiello, and K. A. Willets, "Super-Resolution Imaging Reveals a Difference Between SERS and Luminescence Centroids," ACS Nano **6**(2), 1839–1848 (2012).
45. M. J. Walter, N. J. Borys, G. Gaefke, S. Höger, and J. M. Lupton, "Spatial Anticorrelation between Nonlinear White-Light Generation and Single Molecule Surface-Enhanced Raman Scattering," J. Am. Chem. Soc. **130**(50), 16830–16831 (2008).
46. D. Sivun, C. Vidal, B. Munkhbat, N. Arnold, T. A. Klar, and C. Hrelescu, "Anticorrelation of Photoluminescence from Gold Nanoparticle Dimers with Hot-Spot Intensity," Nano Lett. **16**(11), 7203–7209 (2016).

## 1. Introduction

With the rapid development in synthesis technique and characterization method, the physical properties of metallic nanparticles (NPs), which may find broad applications in various fields of science and technology, have attracted great interest and received intensive studies in the last two decade. The excitation of surface plasmon resonances (SPRs) in metallic NPs, which in turn lead to significant enhancement in electric field near the surfaces of metallic NPs, plays a crucial role in various practical applications [1,2]. The significant enhancement in local electric field can be utilized to enhance the interaction between materials and light. A typical example is the detection of the Raman scattering of single molecules which has been significantly enhanced by SPRs [3–5]. Owing to their superior physical and chemical properties, gold nanoparticles (GNPs) of various shapes have been the focus of many studies [6–11]. In particular, much effort has been devoted to gold nanorods (GNRs) which possess very strong longitudinal SPRs [12,13]. The significantly enhanced two-photon-induced luminescence (TPL) of GNRs, which exhibits strong polarization and wavelength dependences, has been successfully employed to realize optical data storage with ultrahigh density [14–17].

It has been revealed both theoretically and experimentally that large enhancement in local electric field can also be achieved in the nanogap between two metallic NPs which are arranged closely [18–21]. The enhancement appears to be more significant between two GNRs which are usually called a gold nano-antenna [22,23]. The plasmonic coupling between GNPs or GNRs further enhances the electric field in the gap and the significantly enhanced electric field in gold nano-antennas has been employed to build nanoscale sensors [24–27]. It has been demonstrated that the TPL of an ensemble of GNRs can also be greatly enhanced by utilizing the plasmonic coupling of GNRs [28].

So far, two physical mechanisms have been proposed to interpret the TPL of GNRs. In the first model [29], an electron in the d band of gold makes a transition to the sp conduction band after simultaneously absorbing two photons. Then, it thermally relaxes to an energy state above the Fermi level and recombines with the relaxed hole leaving in the d band, giving rise to TPL. Since the transition is initiated by the simultaneous absorption of two photons, a slope close to 2.0 is expected in the dependence of the TPL intensity on the excitation intensity plotted in a logarithmic scale. In the second model [30–32], however, it is suggested that the transition of the electron from the d band to the sp conduction band is realized by sequentially absorbing two photons through an intermediate state.

Very recently, a new mechanism was proposed for the hot luminescence emitted by the hot spots created on the rough surfaces of gold and silver films [33]. It was found that such hot spots can emit efficiently both up- and down-converted hot luminescence under the excitation of femtosecond (fs) laser pulses. By carefully examining the dependence of the hot luminescence intensity on the excitation intensity for single hot spots, it is suggested that the slope derived from the excitation-intensity-dependent hot luminescence should be linearly proportional to photon energy. Different from the physical mechanisms proposed previously [29–32], the hot luminescence from such hot spots originates from the black-body emission of

Optics EXPRESS

hot electrons generated by intraband transition. The hot luminescence was confirmed to originate from the intraband transition of electrons by using excitation photon energy much smaller than half of the bandgap energy of silver. In addition, the hot luminescence spectrum can be well described by black-body emission formula with a high temperature for electrons, further verifying the nature of hot luminescence. Similar intraband hot luminescence was also observed in silver nanorods [34].

Previously, Huang et al. reported the synthesis of hexagonal close-packed gold nanostructures [35]. In this work, we synthesized a novel nanomaterial, which looks like gold nanoflowers (GNFs), by using a different method. Actually, each GNF is formed by the self-assembling of a large number of small GNPs. As a result, there exist many nano-gaps in a GNF where strongly localized modes (i.e., hot spots) may be created. It was shown that efficient hot luminescence could be generated by such GNFs under the excitation of fs laser pulses. More interestingly, we showed that the appearances of such hot spots depend strongly not only on the polarization but also on the wavelength of the excitation light. This characteristic offers us the opportunity and flexibility to selectively excite the hot spots located at different positions, which is quite useful for realizing multi-dimensional optical data storage. As an example of practical applications, we demonstrated the use of such GNFs for realizing multi-dimensional optical data storage with high density and low energy.

## 2. Experimental details and numerical methods

### *2.1 Sample preparation*

In fact, the GNFs described in this work were obtained occasionally in the fabrication of GNRs with copper (Cu) doping. Therefore, the fabrication process can be divided into three steps. The first step is the synthesis of $Cu_2O$ quantum dots. During this process, a certain amount of copper acetate and ethylene glycol was mixed with 10-mL durene. The mixture was put into a Teflon-lined autoclave which was kept at 180°C in a bake oven for 12 hours and then cooled to room temperature in air. Then, the resultant of reaction (i.e., $Cu_2O$ quantum dots) was separated from durene and dispersed in 20% triethanolamine. The second step is actually the same as the conventional procedure for the fabrication of GNRs without any doping. In this case, a little NaCl was firstly added in 5-mL CTAB solution followed by adding $HAuCl_4$ (500 μL, 0.005 M), $AgNO_3$ (32.5 μL, 0.01 M), VC (0.1 M), and $NaBH_4$ (5 μL, 1.67 mM) solutions. Then, the mixture was stirred continuously and kept in water bath at 30°C for 30 minutes. In the final step, the GNRs obtained in the second step were also placed in water bath at 30°C for another 10 hours. Then, 5-μL solution of the above $Cu_2O$ quantum dots was added in the solution of GNRs and stirred for 2 minutes. The mixture was kept in water bath at 22°C for 10 hours and treated with an ultrasonic wave of 300 W for 30 minutes, leading to the formation of GNFs. The GNF-PVA films were made by uniformly dispersing GNFs into a 5% PVA solution, dropping and drying quickly the solution on glass slides.

Physically, the effect of Cu doping is to modify significantly the mechanical stability of GNRs, making them quite fragile. This is because that Cu-Au bond is much weaker than Au-Au bond. As a result, only GNPs with feature sizes of several nanometers can be obtained. Such GNPs possess very large surface energy and they are easily self-assembled into GNFs [36–38]. The doping concentration of Cu is quite small (~0.2%) and Cu has negligible influence on the morphology and photoluminescence properties of the formed GNFs.

### *2.2 Experimental setup*

For the measurement of the hot luminescence of GNFs, the fs laser light delivered by a Ti: sapphire oscillator (Mira 900S, Coherent) with a duration of ~130 fs and a repetition rate of 76 MHz was introduced into an inverted microscope (Observer A1, Zeiss) and focused on the GNF-PVA film by using an objective with NA = 0.85 (60 × ). The hot luminescence of the GNFs was collected by using the same objective and directed to a spectrometer (SR500i-B1,

Optics EXPRESS

Andor) for analysis. A band filter with a narrow spectral width of ~20 nm was used to filter out the excitation light while allowing the detection of both the up- and down-converted hot luminescence. For optical data recording and readout, the GNF-PVA film was placed on a three-dimensional positioning system (P-563.3CD, Physik Instruments) with an accuracy of 1 nm in all dimensions. The fs laser light was fixed while the GNF-PVA film was moved by the positioning system. The hot luminescence generated by the GNF-PVA film was collected by using the objective and directed to a spectrometer (SR500i-B1, Andor) equipped with a photomultiplier tube (H7244-40, Hamamatsu) for analysis. The output signals from the photomultiplier tube were directed to a data acquisition system (BNC-2120, NI) after passing through a lock-in amplifier (SR850, Stanford). A combination of a half-wavelength plate and a quarter-wavelength plate was employed to adjust the polarization of the fs laser light in the plane of the GNF-PVA film. A mechanical shutter was used to control the exposure time of the fs laser light during the processes of data recording and readout. For each information unit, the time for data recording and readout was set to be 20 ms which can be reduced by replacing the mechanical shutter with an acousto-optic modulator. A software was developed to control the synchronous operation of the mechanical shutter, the positioning system and the data acquisition system. A pattern that had been recorded in the GNF-PVA film could be extracted by setting appropriate threshold intensity in the data readout process.

### *2.3 Numerical modeling*

The finite-difference time-domain (FDTD) software developed by Lumerical Solutions, Inc. (http://www.lumerical.com) was employed to simulate the distribution of the hot spots presented in a typical GNF and to obtain the extinction spectrum of the GNF [39,40]. The polarization and wavelength sensitivities of the hot spots were also investigated based on the calculation of the electric field distributions on the GNFs by using the FDTD simulation in which a non-uniform grid with the smallest grid of 0.2 nm and perfectly matched layer condition were employed.

## 3. Results and discussion

### *3.1 Morphology of GNFs*

The morphology of the synthesized GNFs was examined by using transmission electron microscope (TEM) observations. The TEM images for typical GNFs are shown in Fig. 1. The insets show the magnified image and electron diffraction pattern for a typical GNF. From the TEM image of a single GNF, one can easily find that the GNF is formed by the self-assembling of many GNPs with random orientations of their crystalline. Thus, each GNF can be considered as a polycrystalline nanostructure. However, the electron diffraction pattern did not show complete Debye-Scherrer rings which are the typical diffraction patterns for a polycrystalline. It implies that the orientations of the constituent GNFs are not completely random in the self-assembled GNF. From the TEM image of GNFs, it can be seen that GNFs are distinct in morphology from GNRs and GNPs with the existence of enormous small gaps, which is crucial for the generation of polarization- and wavelength-sensitive hot spots. It will be shown that this unique feature is the key factor for realizing multi-dimensional optical data storage.

Optics EXPRESS

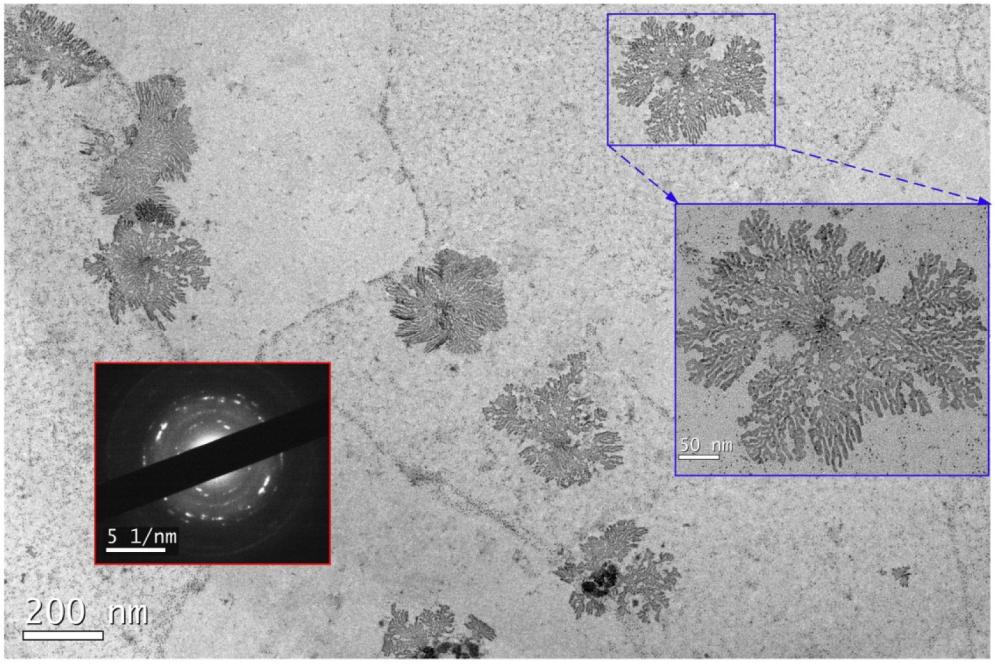


Fig. 1. TEM image of GNFs. The magnified image and electron diffraction pattern for a typical GNF are provided in the insets.

### 3.2 Extinction spectra of GNFs

The extinction spectrum of a large number of GNFs dispersed in water was characterized and a typical one is presented in Fig. 2. One can see two resonant peaks in the extinction spectrum of GNFs, which is quite similar to that of GNRs. The small peak appears at ~510 nm while the large one appears at ~940 nm. It is noticed that the long-wavelength peak at ~940 nm appears to be broad with a large linewidth (full-width at half maximum) of more than 260 nm. In addition, its intensity is more than 3 times stronger than that of the short-wavelength one at ~510 nm. It is thought that the short-wavelength peak originates from the residual GNPs while the long-wavelength one arises from GNFs self-assembled from GNPs. In order to make a comparison with the experimental observation, we have calculated the extinction, scattering and absorption spectra of a typical GNF which is shown in the inset of Fig. 1. The morphology of the GNF was made to be the same as that of the real one while the thickness of the GNF was chosen to be ~2 nm, which is the typical diameter of the GNPs observed in the TEM image. As shown in Fig. 3, a broad extinction band is also observed in the near infrared spectral range. It is noticed, however, that the calculated extinction spectrum appears to be broader than the measured one although it shows a peak at ~900 nm. This is because that the measured spectrum includes the contributions of a large number of GNFs with different morphologies. We also examined the extinction spectra at two different polarization angles of 0° and 90° and found they appeared to be quite similar, as shown in Fig. 3. It is also noticed that the extinction of the GNF is dominated mainly by absorption over the entire spectral range.

Optics EXPRESS

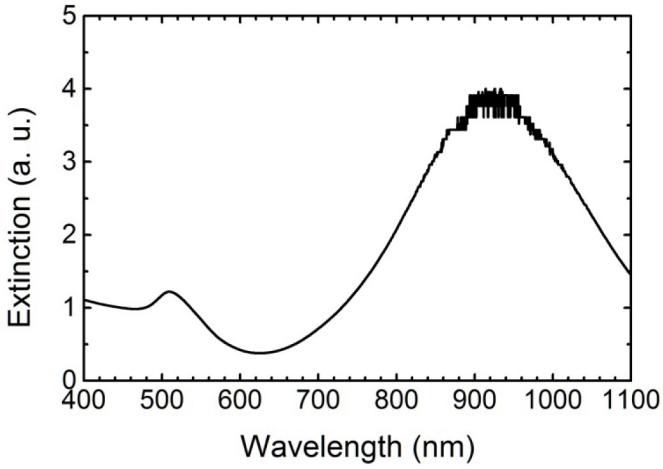


Fig. 2. Extinction spectrum of GNFs dispersed in water.

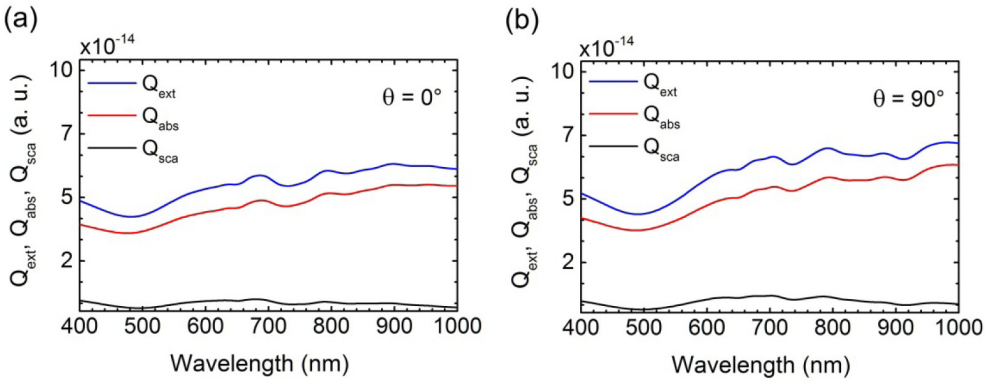


Fig. 3. Extinction ($Q_{ext}$), absorption ($Q_{abs}$) and scattering ($Q_{sca}$) spectra of a typical GNF calculated for an incident light with polarization angles of (a) 0° and (b) 90°.

### *3.3 Polarization and spectrum sensitivities of GNFs*

In order to gain a deep insight into the physical origin for the broad extinction band appearing in the near infrared spectral range, we have calculated the electric field distribution on a typical GNF whose image is shown in the inset of Fig. 1. The dependence of the electric field distribution on the polarization and wavelength of the excitation light is also examined. In Fig. 4(a), we show the electric field distribution on the GNF excited by using a horizontally-polarized plane wave (i.e., θ = 0°) at 800 nm. One can see many hot spots with significantly enhanced electric field which are randomly distributed on the GNF. The maximum enhancement factor in electric field for such hot spots can be as large as ~20. Since the up-converted hot luminescence is generally proportional to the fourth power of the electric field enhancement factor [41–43], an enhancement factor as large as ~$20^4$ is expected for the up-converted hot luminescence intensity. Although the GNPs around the hot spots are only a small fraction of the constituent GNPs for the GNF, they contribute mainly to the extinction of the GNF. When the GNF is illuminated by a vertically-polarized plane wave (i.e., θ = 90°), however, it is found that the appearance of hot spots is completely changed while the maximum enhancement factor remains nearly the same, as shown in Fig. 4(b). It implies that the hot spots depend strongly on the polarization of the excitation light. In Figs. 4(c) and 4(d), we show the electric field distributions calculated for the same GNF excited by a plane wave

Optics EXPRESS

at 750 nm with two different polarizations (i.e., θ = 0° and 90°). It is observed that hot spots on the GNF appear at different positions, implying that they are also sensitive to the wavelength of the excitation light. In Fig. 4, we enclosed the hot spots with top five enhancement factors and marked them with numbers of 1, 2, 3, 4 and 5. It can be seen that the top five hot spots appear at different positions when either the polarization or the wavelength of the excitation light is changed. The polarization- and wavelength-dependent hot spots presented in GNFs are quite useful for realizing multi-dimensional optical data storage, as demonstrated in the following.

It is noticed that the density of hot spots in a GNF is quite large as compared with the low-density hot spots intentionally created on the rough surfaces of gold (Au) and silver (Ag) films [33], making it difficult to map the luminescent hot spots. A recent study revealed the spatial anti-correlation between the two-photon-induced white light and Raman scattering for Ag nanoparticle substrate used to realize electric field enhancement [44]. Similar spatial anti-correlation was also observed in Ag aggregates [45]. Moreover, a reduction of photoluminescence was found in dimers of bipyramids when the electric field intensity of the hot spot was enhanced [46]. Physically, it is thought that the strong wavelength dependence of hot spots, which is also observed in the GNFs discussed in this work, may be responsible for the spatial anti-correlation found in rough Ag substrates or Ag aggregates. It is noticed that the excitation wavelength for the two-photon-induced white light and Raman scattering signal were different in Ref. 44. In Ref. 45, it was thought that the Raman scattering and luminescence are coupled to local plasmon mode and all active plasmon modes respectively, leading to the observed offset between the two signals. For the hot luminescence observed in GNFs, it is thought that the luminescence hot spots appear at the positions while the electric field is significantly enhanced (see Fig. 4), similar to those observed in previous studies on the two-photon-induced luminescence (TPL) of GNRs and gold nanoprisms [41–43].

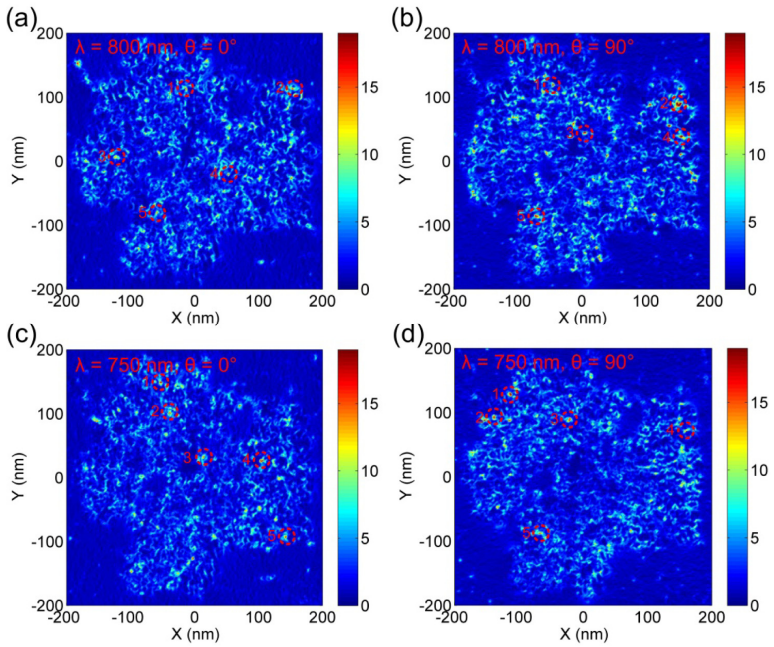


Fig. 4. Electric field distribution on the GNF calculated for an incident light at 800 nm with polarization angles of (a) 0° and (b) 90°, respectively. (c) and (d) show the electric field distributions of the same GNF calculated for an incident light at 750 nm with polarization angles of 0° and 90°, respectively. In each case, the hot spots with top five enhancement factors for electric field are enclosed by dashed circles and marked by numbers of 1, 2, 3, 4, and 5, respectively.

Optics EXPRESS

### 3.4 Characterization of GNF-PVA films

For characterizing the optical properties of GNFs, we uniformly dispersed them in a PVA film. The photo of a typical GNF-PVA film is shown in the inset of Fig. 5. In Fig. 5, we show the transmission spectrum of the GNF-PVA where one can see two valleys at ~510 and ~940 nm. They correspond to the two resonant peaks observed in the extinction spectrum of GNFs dispersed in water. The attenuation of the incident light appears to be different at different positions, implying that the film thickness was not so uniform.

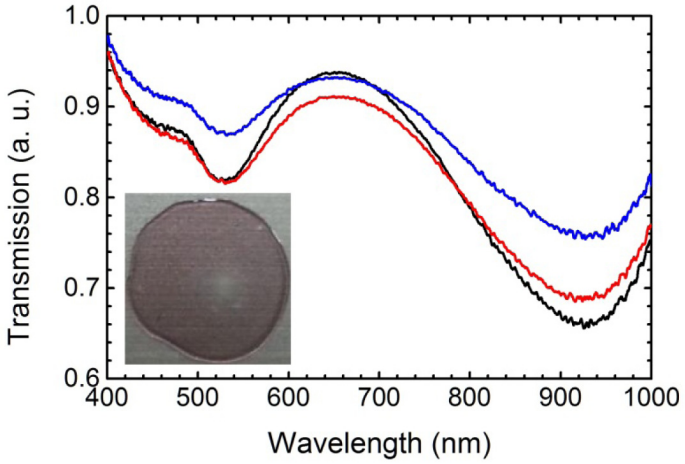


Fig. 5. Transmission spectrum measured at different locations of the GNF-PVA film whose picture is shown in the inset.

### 3.5 Hot luminescence of GNFs

As reported very recently, plasmonic hot spots formed on the surfaces of rough Au or Ag films can emit hot luminescence spanning the visible to near infrared spectral range under the excitation of fs laser pulses [33]. Both the up- and down-converted luminescence can be observed. The physical mechanism for the generation of hot luminescence is completely different from that proposed previously for TPL [29–32]. It involves mainly the intraband transition in both the absorption and emission processes. The hot luminescence originates from the black-body emission of hot electrons whose temperature can be as high as several thousand Kelvin. The key characteristic of such hot luminescence is that for single hot spots the slope derived from the excitation-intensity-dependent luminescence intensity is proportional to the photon energy. However, this feature is lost for an ensemble of hot spots because the electromagnetic environments for different hot spots are different.

Here, the hot spots generated in the GNFs are quite similar to those observed on the surface of rough Au films, as can be seen in Fig. 4. They are basically strongly localized electric modes generated in the narrow gaps of GNFs. Since the density of such hot spots is quite large, it is difficult to characterize the hot luminescence of a single hot spot. For this reason, we examined only the hot luminescence generated by many GNFs dispersed in a PVA film because the diameter of the excitation spot is several microns.

Optics EXPRESS

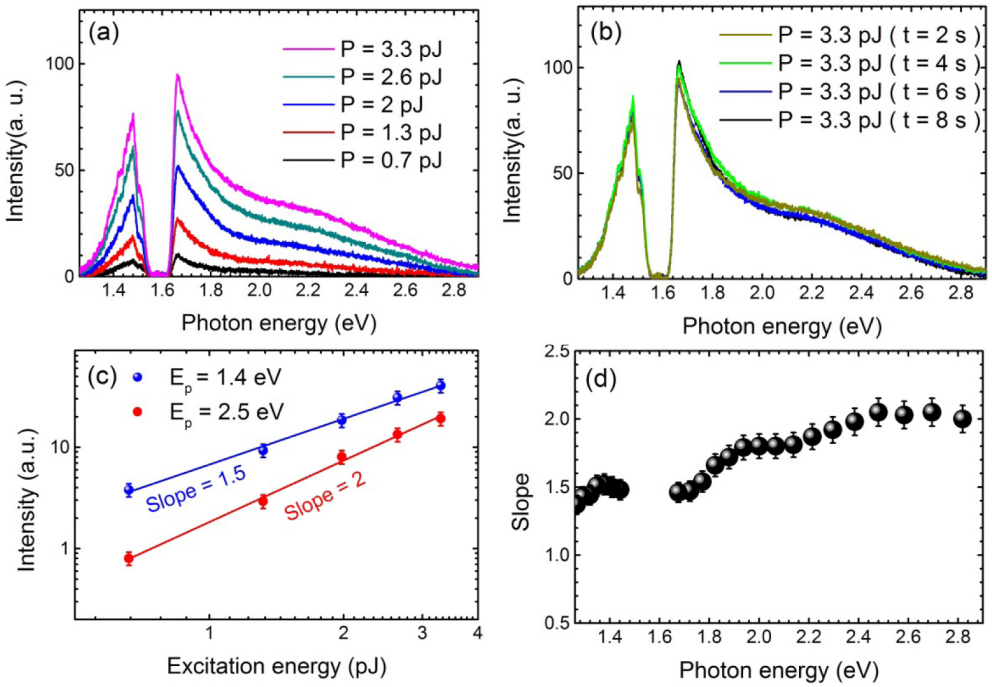


Fig. 6. (a) Hot luminescence spectra of the GNF-PVA film measured at different pulse energies. (b) Hot luminescence spectra measured at pulse energy of 3.3 pJ and different times. (c) Dependence of the luminescence intensity on the excitation pulse energy plotted in a double-logarithmic coordinate for two photon energies. (d) Slopes derived from the dependence of the luminescence intensity on the excitation pulse energy shown in (a) at different photon energies

In Fig. 6, we show the evolution of the hot luminescence spectrum with increasing excitation pulse energy (P) measured at 785 nm. The excitation light was almost filtered out by using a bandpass filter. The maximum excitation pulse energy was chosen to be ~3.3 pJ at which no photomodification was observed, as can be seen in Fig. 6(b) where the hot luminescence spectrum does not change with time. On both sides of the excitation photon energy, we can observe the down-converted and up-converted luminescence, which is quite similar to that observed for rough Au or Ag films [33]. At each wavelength (or photon energy $E_p$), we can plot the hot luminescence intensity as a function of the excitation pulse energy in a double logarithmic coordinate which generally shows a straight line [see Fig. 6(c)]. The slopes of the straight lines at different photon energies have been derived and presented in Fig. 6(d). A linear dependence of the slope on the photon energy, which is the characteristic of a single hot spot, is not observed because we were examining a huge number of hot spots. Different from the hot luminescence emitted from single hot spots on Au or Au films, which exhibits a slope proportional to the photon energy [33], we found that the slope derived at any photon energy is almost proportional to the luminescence intensity at this photon energy. Consequently, the derived slope as a function of photon energy appears to be quite similar to the spectrum of the hot luminescence, as shown in Fig. 6.

We also measured the up-converted luminescence under different excitation wavelengths. The excitation-wavelength-dependent spectra measured at the same pulse energy of 9.9 pJ are presented in Fig. 7. With increasing excitation wavelength, an increase in the luminescence intensity is observed. This trend is in good agreement with that predicted from the extinction spectrum shown in Fig. 2 or the transmission spectrum shown in Fig. 5. Owing to the large electric field enhancement achieved at the hot spots, the up-converted luminescence is quite efficient even at very low pulse energies. The signal to noise ratio at the excitation

Optics EXPRESS

wavelength of 760 nm is sufficient for realizing optical data storage. For longer excitation wavelengths, lower pulse energies for optical data storage are expected.

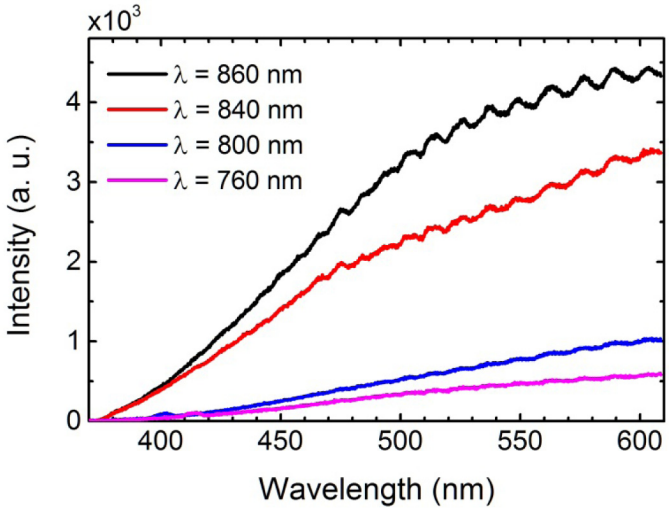


Fig. 7. Up-converted hot luminescence of the GNF-PVA film measured at the same pulse energy of 9.9 pJ under different excitation wavelengths.

### *3.6 Optical data storage realized by using GNF-PVA films*

As shown in Fig. 5, the extinction (or absorption) spectrum of the GNF-PVA film appears to be a broad band. In addition, the hot luminescence emitted by GNFs is quite efficient even at 760 nm where the extinction (or absorption) of GNFs is not so large because of the significantly enhanced electric field at hot spots. This feature offers us the opportunity to realize wavelength multiplexing with more wavelength channels. In addition, the annihilation of the hot spots at one wavelength has negligible influence on the hot spots at the other wavelengths, implying much better isolation between different wavelength channels. These two characteristics make it possible to achieve wavelength multiplexing with a small wavelength separation over a broad wavelength region which will significantly increase the density of optical data storage.

The strong polarization and wavelength dependence of the hot luminescence observed in GNFs, which originates from the strong polarization and wavelength dependence of the hot spots, offers us the possibility of using them to realize multi-dimensional optical data storage media with ultrahigh density. In order to demonstrate feasibility of such an idea, we have fabricated GNF-PVA films in which GNFs are uniformly distributed, as shown in the inset of Fig. 5.

To demonstrate the use of two orthogonal polarizations in the recording and readout of optical data, we recorded two patterns with letters “A” and “B” by using two orthogonal polarization angles of 0° and 90° and the extracted patterns by detecting the up-converted luminescence are shown in Fig. 8. Each pattern was decomposed as a binarized image composed of 100 × 100 pixels with a size of 1.0 × 1.0 $\mu m^2$. The wavelength of the fs laser light was set at 800 nm and the irradiation time was chosen to be 10 ms. The pulse energy for recording and readout were chosen to be 9.9 and 2.5 pJ, respectively. Basically, we can use correlation coefficient (C) to characterize the quality (or error rate) of an extracted pattern. It is defined as follows:

Optics EXPRESS

$$C = \frac{\sum_m \sum_n (A_{mn} - \overline{A})(B_{mn} - \overline{B})}{\sqrt{\left[(A_{mn} - \overline{A})^2\right]\left[(B_{mn} - \overline{B})^2\right]}} \quad (1)$$

where $\overline{A} = \frac{\sum_m \sum_n A_{mn}}{m \times n}$, $\overline{B} = \frac{\sum_m \sum_n B_{mn}}{m \times n}$. $A_{mn}$ and $B_{mn}$ represent the intensities of individual information units ($m$, $n$) while $\overline{A}$ and $\overline{B}$ denote the averaged intensities of all the information units in the extracted and original patterns, respectively. Another parameter that characterizes the quality of the extracted pattern is contrast (R) which is defined as $R = (I_1 - I_2)/(I_1 + I_2)$. Here, $I_1$ and $I_2$ denote the averaged intensities of all the information units without and with the irradiation of fs laser pulses.

In Figs. 8(a) and 8(b), the correlation coefficient (C) and contrast (R) of the extracted pattern were calculated to be ~0.91 and 0.39 (or 0.90 and 0.40), respectively. It is noticed that no cross-talk was observed for the two patterns recorded and extracted by using the two orthogonal polarization angles, indicating that the isolation between different polarization channels achieved by using GNFs is comparable or even better as compared with GNRs. Another remarkable feature is the low pulse energy used for data recording, which was only 9.9 pJ. As compared with the pulse energy reported in the previous literature [16], a significant reduction in pulse energy was achieved. Consequently, no obvious change in the morphology of the GNF-PVA films was found before and after data recording, as shown in Fig. 9.

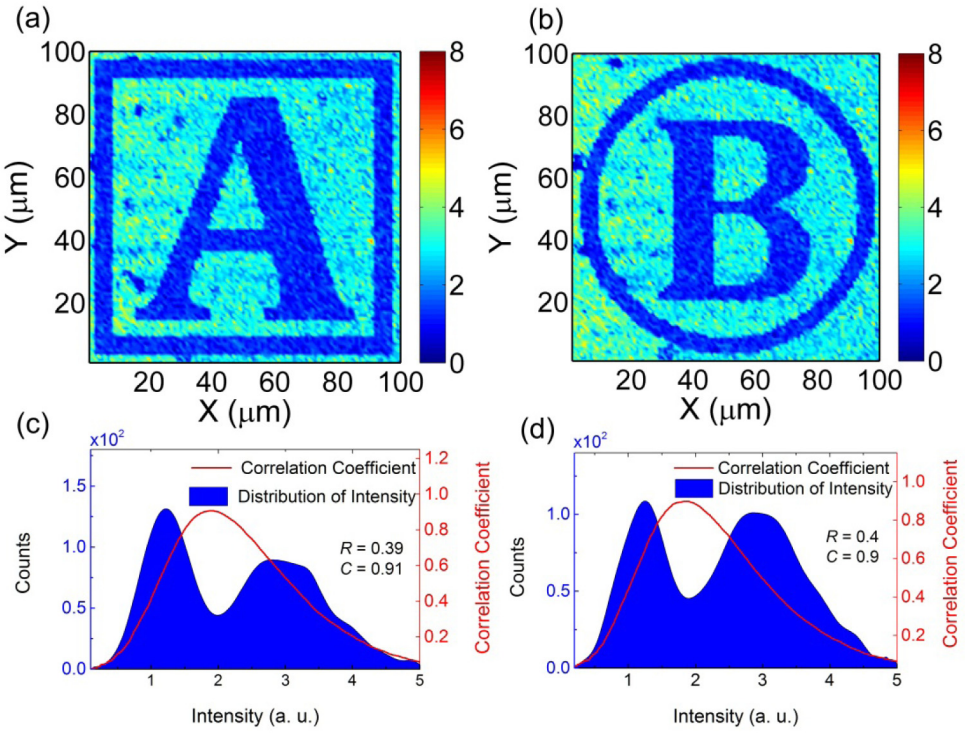


Fig. 8. Patterns recorded and extracted by using (a) horizontally- and (b) vertically-polarized fs laser light at 800 nm. The pulse energies used for data recording and read out were 9.9 and 2.5 pJ, respectively. The statistics of the luminescence intensities of all the pixels for the two patterns shown in (a) and (b) are presented in (c) and (d), respectively. The correlation coefficients (C) and contrasts (R) calculated for the two extracted patterns are also provided.

Optics EXPRESS

In order to find out how many polarization channels can be achieved in optical data storage, we have tried to record and extract three patterns by using three polarization angles of 0°, 60°, and 120°, as shown in Fig. 10. In this experiment, linearly polarized fs laser light with polarization angles of 0°, 60° and 120° was employed in the data recording and readout processes. Although a small cross-talk can be identified, it has little effect on the quality of the extracted patterns. It implies that three polarization channels separated by 60° can be realized with a tolerable cross-talk. This result is comparable to the storage media made of GNRs [16].

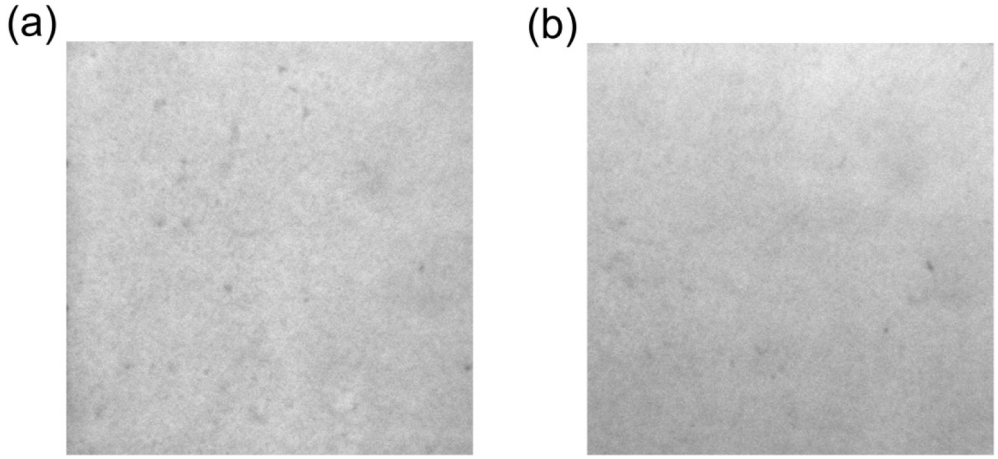


Fig. 9. Morphologies of the (a) left-up and (b) right-bottom corners of the GNF-PVA film after the recording and readout processes.

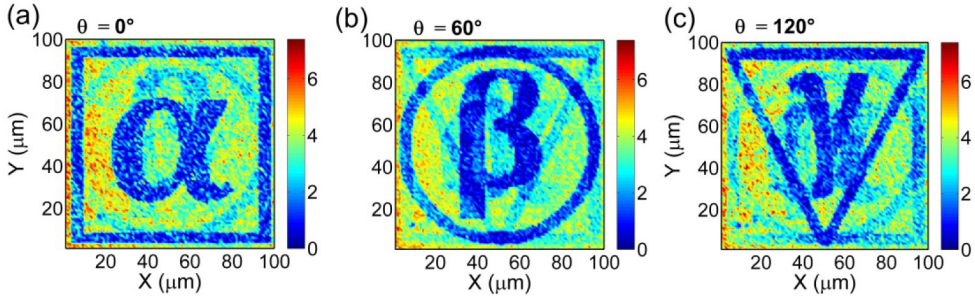


Fig. 10. Patterns recorded and extracted by using fs laser light with a wavelength of 800 nm and polarization angles of (a) 0°, (b) 60°, and (c) 120°, respectively. The pulse energies used for recording and readout were 2.6 and 0.65 pJ, respectively.

Apart from polarization multiplexing, we also examined the wavelength multiplexing of the fabricated GNF-PVA films in optical data storage and the results are shown in Fig. 11. Data recording and readout were characterized in two wavelength channels separated by only 40 nm (i.e., $\lambda$ = 800 and 760 nm). Although a small cross-talk was observed, it is still tolerable from the viewpoint of practical application. The narrow wavelength separation between neighboring channels in combination with the broad extinction spectra of the GNF-PVA films make it possible to realize more wavelength channels with negligible cross-talk, further enhancing the capacity of the storage media based on GNFs.

Optics EXPRESS

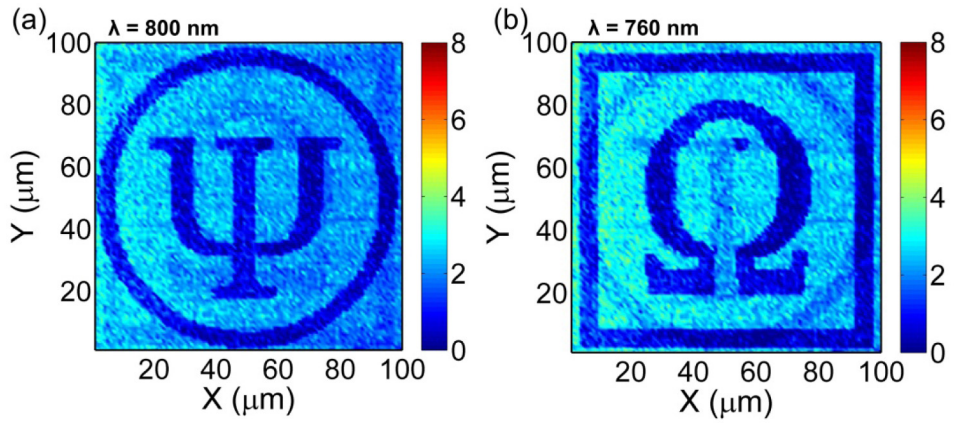


Fig. 11. Patterns recorded and extracted by using a horizontally-polarized fs laser light with wavelengths of (a) 800 nm and (b) 760 nm, respectively. The pulse energies used for recording and readout were 3.3 and 0.8 pJ, respectively

## 4. Conclusion

In summary, we have fabricated GNFs which are self-assembled from GNPs by adding $Cu_2O$ quantum dots into the synthesis process of GNRs. The as-prepared GNFs exhibit broad extinction spectra spanning the visible to near inferred spectral range. Polarization and spectrum sensitive hot spots with significantly enhanced electric field were found to exist on the surfaces of such GNFs. The GNFs could emit very efficient up- and down-converted hot luminescence under the excitation of fs laser pulses. The slope derived from the dependence of the hot luminescence intensity on the excitation energy exhibits a spectrum quite similar to the spectrum of the hot luminescence, which is clearly distinct from the behavior of single hot spots created on the surfaces of rough Au and Ag films reported previously. As a possible application, we demonstrated experimentally that the polarization- and wavelength-dependent hot luminescence could be employed to realize optical data storage with high-density and low energy.

## Funding

National Natural Science Foundation of China (NSFC) (Grant No. 11374109, 11674110, 61201102); Natural Science Foundation of Guangdong Province, China (Grant. No. 2016A030308010); Science and Technology Planning Project of Guangdong Province, China (Grant No. 2015B090927006).